Fast and efficient chromium(VI) extraction by colloidal Mg/Al layered double hydroxide nanoparticles

Abdelhak Fezraoui, Damien Cornu, Marc Hébrant

Fast and efficient Chromium(VI) extraction by colloidal Mg/Al Layered Double Hydroxide nanoparticles.

A. Fezraoui, D. Cornu*, M. Hébrant

Laboratoire de Chimie Physique et Microbiologie pour l'Environnement (LCPME), CNRS and Université de Lorraine, UMR7564, 54600, Villers-lès-Nancy, France

* Corresponding author : Laboratoire de Chimie Physique et Microbiologie pour l'Environnement (LCPME), CNRS and Université de Lorraine, UMR7564, 54600, Villers-lès-Nancy, France

E-mail address : damien.cornu@univ-lorraine.fr

Graphical abstract

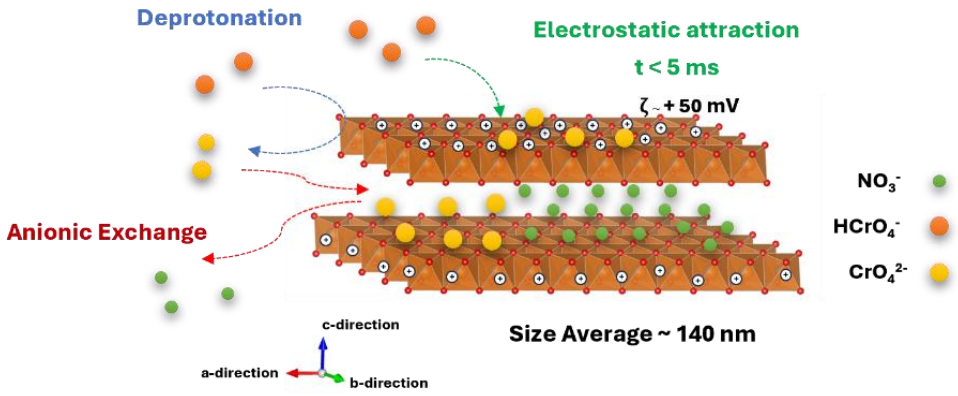

Keywords:

Layered double hydroxides, Colloid, Hexavalent chromium, Stopped-flow kinetics, Ultrafiltration, Anion exchange, Extraction.

Abstract:

Due to the constraints associated with diffusion and mixing time, traditional kinetic and thermodynamic approaches were inadequate for probing the true mechanism of interaction between chromate and Layered Double Hydroxide (LDH). To circumvent these limitations, colloidal suspensions of Mg/Al-NO_3 LDH, characterized by a positively charged surface (approximately +50 mV) in ultrapure water and a mean average diameter of 140 nm, allowing the formation of stable suspensions for days, were swiftly mixed with Cr(VI) suspensions at both pH = 4 and 9 using a stopped flow technique. This rapid mixing, accomplished in less than 5 milliseconds, enabled the examination of the initial stages of interaction between the toxic anion and the host compound. Two distinct steps in the adsorption process were identified: a very fast step (completed in less than 5 ms), representing up to 80% of the measured variation, and a slower step lasting up to 100 s. The fast step assumed to be driven by electrostatic interaction ($\zeta \sim +50$ mV) with the surface, and sites close to the surface are easily accessible to the chromate anions. The slower step corresponded to a diffusion process close or inside the particles. Chromate extraction efficiency was investigated through ultrafiltration tests, varying the LDH and chromate amounts, indicating that 2 nitrate ions are exchanged for 1 chromate, regardless of the pH considered, and a total exchange can be fulfilled with 0.1 g L^{-1} of LDH within the explored concentration range.

Introduction :

Chromium (Cr) is extensively utilized in various industrial processes, including metallurgy for the production of stainless steel, ensuring its "stainless" quality (Barnhart, 1997). Additionally, it finds applications in tanneries, electroplating, wood preservation, and refractory industries (Ukhurebor et al., 2021). However, these industrial activities often result in the release of Cr into downstream effluents. In aqueous environments, hexavalent chromium (Cr(VI)), is highly toxic, and carcinogenic (Islam et al., 2019). The World Health Organization recommendations has set a maximum acceptable limit for total Cr in drinking water at 50 ppb (Vaiopoulou and Gikas, 2020).

Therefore, efficient removal of Cr(VI) from aqueous effluents is imperative, and various methods are studied/developed for this purpose, including adsorption (Yuan et al., 2013), membrane processes (Mantel et al., 2022), ion exchange (Verma and Sarkar, 2020), chemical precipitation (Xie et al., 2017), and flocculation/coagulation (El Gaayda et al., 2023). Among these techniques, adsorption stands out as a widely recognized and economically favorable method (Lei et al., 2017). The appeal of adsorption lies in its numerous advantages, including high removal efficiency, straightforward design, low operational costs, minimal risk of causing secondary pollution, and the ability to separate a diverse range of pollutants from water media (Qin et al., 2020; Tran et al., 2019). The versatility and cost-effectiveness of adsorption make it a preferred choice in addressing the challenges associated with Cr(VI) contamination in aqueous environments.

Layered double hydroxides (LDH) are a class of materials that exhibit significant potential as inorganic scavengers. One of their notable attributes is their ability to achieve a high anion exchange capacity (Chubar, 2011; Tran et al., 2019). LDH compounds are layered materials characterized by their unique chemical formula $[M^{II}_{1-x}M^{III}_{x}(OH)_2]^{x+}[A^{n-}]_{x/n}.yH_2O$. M^{II} denotes bivalent metal cations and M^{III} represents trivalent metal cations, both located in layers, binding hydroxide anions arranged in octahedra units. A^{n-}, the interlayer anions, is located in the interlayer space, weakly bonded to the layers and therefore easily exchangeable. The absence of crosslinking between the octahedral brucite-like layers in LDH is a notable characteristic that allows for the expansion or contraction of the interlayer spacing to accommodate a wide range of interlayer anions (Goh et al., 2010; Goh and Lim, 2010; Hsu et al., 2007).

The extensive reviews conducted on Cr(VI) adsorption on LDH consistently recommend it as a potential adsorbent, either in its single or composite forms (Ahmed and Mohamed, 2023; Dong et al., 2022; Feng et al., 2022; Goh et al., 2008; Guan et al., 2022), with co-adsorbents including polymers (Zhu et al., 2016), activated carbon (Zhang et al., 2022), clay minerals (Jarrah et al., 2020), metal-organic frameworks (Wang and Guo, 2019), and iron oxides (Miao et al., 2021). Recent research efforts have explored the adsorption mechanisms of hexavalent chromium (Cr(VI)), with Tran et al. (Tran et al., 2019) identifying three potential mechanisms for LDH in their review on adsorption.

These proposed mechanisms involve electrostatic attraction between the chromate ion and the positively charged surface of the particles, anion exchange, and adsorption-coupled reduction of Cr(VI) to Cr(III) followed by incorporation of the trivalent generated cation onto LDH-based materials. The temporal aspects and the relative significance of these mechanisms are not adequately detailed in the literature.

Electrostatic attraction between Cr(VI) and the positively charged LDH surface is considered a crucial mechanism in the LDH-Cr(VI) interaction. Chao et al. (Chao et al., 2018) reported that these positive potentials are attributed to the prevalence of hydroxyl groups on the outer surface of the LDH, which attract H^+ protons, leading to the formation of positively charged groups known as $-OH_2^+$. Once attracted to the surface of the particles, Cr(VI) anions will either be exchanged or stay in the vicinity of the surface.

The second mechanism, anion exchange, plays a crucial role in capturing Cr(VI) species from aqueous solutions, as demonstrated in a study conducted by Goh and Lim. They investigated the adsorption of toxic oxyanions and how the presence of other coexisting anions influenced adsorption efficiency, particularly in alkaline conditions (pH 8-11.5) (Goh and Lim, 2010). They have shown that this efficiency was correlated to the ionic potential, a value calculated based on their ionic radius and ionic charge ranging between 4.67 to 10.81 nm^{-1}, the larger the ionic potential, the easier the insertion of the anion in the structure. With a value of 8.33 nm^{-1}, chromate is more likely to be inserted as nitrate (5.00 nm^{-1}). However, chromate was still captured in the LDH even with large concentrations of competing anions with larger ionic potentials such as sulfate (8.70 nm^{-1}) and carbonate (10.81 nm^{-1}).

The third reported possible mechanism associated with the reduction of Cr(VI) to Cr(III) in LDH-based materials using reducing agents such as the biomass or as Fe(II) (Lv et al., 2019; Wani et al., 2021).

The derived conclusions stem from a comprehensive investigation into the kinetics of interactions between Cr(VI) and LDH-based materials, involving a thorough literature review spanning the years 2004 to 2022. This scrutiny encompassed an in-depth examination of adsorption kinetics and isotherms across various time intervals, ranging from 0 to 20 minutes up to 50 hours. Furthermore, equilibrium times were explored, varying from 5 minutes to 24 hours. These variations were attributed to the diverse array of composite materials utilized (Tran et al., 2019). A profound understanding of the interaction mechanism between Cr(VI) and LDH holds the key to develop reusability and regeneration processes without compromising the physicochemical characteristics of LDH materials (Mubarak et al., 2018). In addition to a diverse array of macroscopic and spectroscopic characterization techniques (Hsu et al., 2019), investigations utilizing electrochemical techniques (Lahkale and Sabbar, 2023) have been crucial in emphasizing the kinetics and mechanisms underlying the interaction between Cr(VI) and LDH materials. However, these studies are limited as the time

scale below 2 minutes cannot be explored by conventional approaches, and most of the adsorption occurs quicker than this time scale. A good understanding of the mechanism is limited by the diversity of the phenomena occurring at short time scale: homogenization of the solution, diffusion towards particles, interaction with the particles and diffusion within the particles.

In this study, LDH nanoparticles with a minimal and homogeneous particle sizes were synthesized to enhance reactivity toward Cr(VI). Nitrate had been chosen as the interlayer anion because it is widely used as exchangeable anion in the literature (Goh et al., 2009), which will allow us to easily compare our results on chromate with other anionic exchange mechanisms. The synthesis yielded a colloidal suspension, facilitating the investigation of the interaction between LDH particles and Cr(VI) up to the millisecond scale using the stopped-flow technique and limiting the diffusion time scale of the reactants to the LDH nanoparticles (NPs). This approach enabled the unraveling of sequences involved in various mechanisms. Furthermore, through the use of the ultrafiltration technique, a thorough exploration of the equilibrium allowed for the determination of the thermodynamic equilibrium constant for the anion exchange mechanism.

Materials & Methods :

1-Materials

Aluminum nitrate nonahydrate ($Al(NO_3)_3 \cdot 9H_2O$, ≥99%), Magnesium nitrate hexahydrate ($Mg(NO_3)_2 \cdot 6H_2O$, ≥99%), and Nitric acid (HNO_3, 65%) were purchased from SIGMA-ALDRICH. Sodium chromate tetrahydrate ($Na_2CrO_4 \cdot 4H_2O$, ≥99.5%) was purchased from LABOSI (Fisher-Scientific). Sodium hydroxide solution (NaOH, 1 mol L^{-1}) was purchased from VWR Chemicals. The standards used for ICP-MS tests were prepared in the laboratory from commercial solutions certified at 1000 ppm (Merck), and Ultrapure water 18.2 $M\Omega.cm^{-1}$ (Elga Water).

2-Synthesis

Mg_2Al-NO_3 LDH NPs synthesis was adapted from a previous work (Awassa et al., 2022). Ultrapure water was used to prepare a 20 mL solution containing mixed metal salts of $Mg(NO_3)_2 \cdot 6H_2O$ and $Al(NO_3)_3 \cdot 9H_2O$ with a molar ratio of Mg/Al = 2 and a total concentration of cations of 1 mol L^{-1}. The prepared solution was then added directly to 40 mL of a 1 mol mol L^{-1} NaOH solution under vigorous stirring and $N_{2(g)}$ purging to minimize carbonate formation in the alkaline reaction medium. After 15 minutes of reaction, the resulting slurry was transferred directly into a 100 mL autoclave made of stainless steel with a Teflon lining and subjected to a 16-hour hydrothermal treatment at 80°C. Following the hydrothermal treatment, was washed with centrifugation for 4 times with 50 mL ultrapure water, and the final solid product of LDH NPs was obtained, which was then dried at 80°C for 4 hours for further characterization. It was worth mentioning that contrary to what was done with

Zn2Al-NO3 NPs, the washing step was preceded by the hydrothermal treatment. Indeed, the solubility of Mg leads to a partial dissolution of the LDH and a subsequent precipitation of undesired $Al(OH)_3$ and a Mg/Al ratio of 3 or 4 in the LDH (see Figure S1 in the Supporting Information (SI)).

3-Characterizations:

Powder x-ray diffraction (PXRD)

The structural investigation of LDH NPs was carried out using a Panalytical X'Pert Pro MPD diffractometer with a Bragg-Brentano geometry equipped with a copper anticathode that generated radiation with a wavelength of Cu ($K_{\alpha 1}$) = 0.15406 nm. The instrument was further enhanced with a Ge(111) incident-beam monochromator, Soller slits of 0.02 rad, and programmable divergence and anti-scatter slits. The sample's irradiated area was fixed at 10 × 10 mm², and data collection employed an X'Celerator detector. To obtain the diffraction pattern, the instrument was set to scan the region between 5 and 80° at a scanning speed of 1° per minute. To improve resolution and minimize preferential orientation of LDH crystallites, the holder rotation rate was fixed at 15 rotations per minute. The lattice parameters of LDH NPs were determined from the analysis of the (003) and (110) basal reflections.

Inductively coupled plasma mass spectrometry

Inductively coupled plasma mass spectrometry (ICP-MS; Agilent-7800) of isotopes ^{26}Mg, ^{27}Al, and ^{50}Cr was used to determine the molar ratio of Mg^{2+}/Al^{3+} in LDH NPs after dissolution in 5% HNO_3 and appropriated dilutions. To construct the calibration curves, a selection of 8 concentration points was chosen. Subsequently, the Cr concentration in the collected permeate samples was determined after suitable dilution in 1% HNO_3. The analysis of the permeate was carried out 2 times with 3 repeated measurements each time. The errors bar given in the results were taken as 3 times the standard deviation of the yield efficiency calculated on the basis of the 6 ICP-MS measurements.

Elementary analysis (CHNS analysis)

The analysis of carbon and nitrogen elements fractions in the solid was conducted using a Thermo Fisher Flashsmart elementary analyzer.

Raman spectroscopy

A Renishaw inViaTM Qontor microspectrometer with an optical microscope in confocal mode, equipped with a long-frontal Olympus X50 objective with a numerical aperture of 0.55 and a slit opening aperture of 0.65 µm was used on the sample, the laser's (λ = 532 nm) power was about 10 mW. The spectra were acquired in 20 acquisitions of 5 seconds each with a spectral resolution of 3 cm^{-1}.

Fourier transform infrared spectroscopy (FT-IR)

The mid-infrared range infrared spectra were obtained using a Bruker Vertex 70v spectrometer, equipped with a KBr beam-splitter and a deuterated triglycine sulfate (DTGS) detector. To acquire the spectra of the LDH NPs powder, an attenuated total reflection (ATR) accessory with a single reflection diamond crystal (Platinum ATR, Bruker) was utilized under vacuum conditions (<1 hPa). The spectral resolution was adjusted to 4 cm^{-1}, and each individual spectrum was acquired by collecting data for 1 minute (equivalent to 100 scans) within the wavenumber range of 4000 - 400 cm^{-1}.

Scanning electron microscopy

In our work, scanning electron microscopy (SEM) was devoted to analyzing the morphology of LDH NPs via a JEOL JSM-IT500HR instrument with an electron beam voltage of 10 kV, performing in high vacuum conditions. Two small drops of a diluted suspension of LDH NPs in ultrapure water were then placed on a copper film and allowed to air dry overnight. The average particle size of the NPs was determined using the ImageJ software by analyzing 100 individual LDH NPs from their SEM images.

Atomic force microscopy

In this study, LDH NPs were photographed in the air utilizing SNL-C tips (Bruker Corporation) in peak-force tapping mode. After being dispersed in an ethanol solution and sonicated for thirty minutes, LDH NPs were applied to clean silicon substrates and allowed to dry overnight at room temperature.

Dynamic light scattering (DLS) and Zeta-potential (ZP)

Zeta-potential and particle size measurements were conducted using a Zetasizer nano-ZS (Malvern Instruments, Malvern, UK) at a temperature of 25°C. Disposable zeta cells were used. For the experiments, a LDH suspension with a concentration of 40 mg L^{-1} was prepared, and its pH was adjusted to different values using small droplets of HNO_3 (0.1 mol L^{-1}) and NaOH (0.1 mol L^{-1}) solutions. Each NPs suspension was then placed in optical quartz cuvette with a path length of 10 mm, and measurements were recorded over time to determine the volume median diameter (D_{v50}) and volume diameter of 90% (D_{v90}) of the NPs.

4-Reactivity of NPs

For all the tests of reactivity, the pH was adjusted to using HNO_3 (0.1 mol L^{-1}) and NaOH (0.1 mol L^{-1}) solutions to weather adjust Cr(VI) solutions or the LDH NPs suspensions.

Ultraviolet-visible spectroscopy

Ultraviolet-visible (UV-Vis) absorption spectroscopy experiments were carried out using a Cary 60 UV-Vis spectrometer (Agilent Technologies). Extinction coefficients and speciation of Cr(VI) in both alkaline and acidic media were determined by constructing calibration curves within the concentration

range of 5 - 25 mg L^{-1}. This method was also applied in the preliminary study of the interaction between Cr(VI) and LDH NPs under both conditions.

Stopped flow technique

The NPs reactivity towards Cr(VI) were studied using a stopped-flow device, Bio-Logic SFM20, with an optical path length of 1 cm. Biokine software (Bio-Logic) was used to coordinate the data collecting and experimental fitting. After preparing the NPs suspension with the proper concentration and pH values, all experiments were carried out at a constant temperature of 25°C. The kinetic traces were collected with a thousand data points optical detector, which was chosen to optimize the signal-to-noise ratio. The dead time of the instrument was determined to be 4.3 ms (Tonomura et al., 1978). The absorbances were monitored at 375 nm, which is one of the characteristic absorption wavelengths of Cr(VI). Each stopped-flow kinetic curve reported represents the mean value obtained through multiple acquisitions (5-10). This approach was adopted to minimize noise and enhance the signal-to-noise ratio, ensuring the reliability and accuracy of the presented kinetic data. The error bars of the obtained fitted kinetic constants (k_{obs}) were taken as three time the standard deviation of the adjusted parameter coming from the fitting procedure.

Ultrafiltration tests

The ultrafiltration system Amicon 8010 (Millipore) equipped with regenerated cellulose membranes (PLGC, 10 kDa, Millipore) was utilized. It took approximately 7 minutes to collect 5 mL of permeate in all experiments. The ultrafiltration membrane having pores typically of around 2.5 nm diameter, the LDH particles in suspension were retained and only the “free” Cr(VI) species in solution and could pass through the ultrafilter. The resulting permeates were obtained through duplicated ICP-MS analyses. The thermodynamic constants underwent a calculation process using Monte Carlo propagation of uncertainty. This process involved calculating different K-constants by systematically eliminating one data point at a time from the residue calculation. Subsequently, an ensemble of K-values was obtained, and the standard deviation of the K-constant was determined using this ensemble.

Solid characterization:

LDH NPs were saturated with a Cr(VI) solution at both pH values. The initial chromium concentration was 500 mg L^{-1}, with a solid concentration of 3.33 g L^{-1}. After saturation, the solid was centrifuged, and its structural stability after the exchange was characterized using PXRD technique.

Results and discussion :

1. Characterization of the LDH-NPs

a. Structure and Purity

PXRD was utilized to evaluate the crystalline nature of the resulting LDH, as shown in Figure 1a. The PXRD plot clearly demonstrated a distinct presence of crystalline structure along the c-direction, evidenced by the (003) and (006) reflections and no significant presence of other crystalline structure. Moreover, the a-direction exhibited a well-defined crystalline structure, notably highlighted by the (110) reflection. Lattice parameters had been determined and are presented in Table 1. For Mg/Al-NO_3 LDH NPs, the lattice parameters (a, c) measured at 3.04 Å and 26.53 Å, respectively. These values closely align with those reported in existing literature for larger Mg/Al-NO_3 LDH particles with a 2:1 ratio, Marappa et al. (Marappa et al., 2013) reported a lattice parameter c of 26.40 Å, and similarly, Xu et al. (Xu and Zeng, 2001) found c = 26.83 Å and a = 3.04 Å, confirming the consistency of the findings.

The Raman spectra is illustrated in Figure 1b shows the key bands at 1056 cm^{-1} $\nu_1(NO_3^-)$ and 717 cm^{-1} $\nu_4(NO_3^-)$, affirming the intercalation of only NO_3^- anions into the LDH layers (Frost and Musumeci, 2006) because carbonate anions have a close but distinct vibration frequency at 1062-1068 cm^{-1}. Moreover, bands at 556 cm^{-1} ($A_{1g}(T)$) and 478 cm^{-1} ($E_{u(T)}$) indicated the presence of octahedral brucite-like layer hydroxyl groups. In alignment with previous research by Di Bitetto (Bitetto, 2017), the investigation of three distinct ratios (ranging from 2 to 4) of nitrated LDH was conducted using Raman spectroscopy, with a specific focus on the intense $\nu_1(NO_3^-)$ band at 1056 cm^{-1}. Showing that, as the molar ratio Mg/Al approaches 3, an additional band emerged at a lower wavenumber, approximately 1046 cm^{-1}. The absence of this additional band in our results indicates an approximate Mg/Al ratio of 2 within the LDH structure.

In the FT-IR spectrum is illustrated in Figure 1c. The broad band, centered around 3386 cm^{-1}, corresponded to the stretching vibration mode of the OH bond of both the hydroxide group within the brucite-like layer and the crystalline water molecules within the interlayer space. The presence of the latter ~~is~~ was supported by the band at 1643 cm^{-1}, which attributed to the bending vibration mode of water molecules residing in the interlayer region. Additionally, a distinct band at 1344 cm^{-1} linked to the antisymmetric stretching vibration $\nu_2(NO_3^-)$ of the interlayer anion NO_3^- (Kloprogge et al., 2002). Moving to the lower frequency range, the heightened bands at 613 cm^{-1} clearly indicates of the existence of metal-oxygen bonds within the octahedral brucite-like layer. These bands can be particularly attributed to the bending vibrations of both O-Mg-O and O-Al-O bonds. These two vibrational techniques provided valuable insights into LDH composition and structures features, confirming the successful incorporation of NO_3^- anions and the effectiveness of the synthesis method.

In addition to the structural study, an elemental analysis of the LDH NPs, once dissolved into nitric acid, has been performed. The chemical analysis results are presented in Table 1 reveal a Mg/Al ratio of 2.01, determined through the ICP-MS technique confirming the achievement of the desired fixed

ratio, and attesting to the success of the synthesis conditions and corroborating the ratio observed with the nitrate band in Raman analysis. Furthermore, the elemental analysis of light elements, performed using CHNS analysis, indicates the successful production of fully nitrated LDH a nitrogen content of 4.1 $mmol.g^{-1}$ of N which was very close to the theoretical value at 3.9 $mmol.g^{-1}$ without the presence of carbon atom and therefore validating the absence of carbonate ions in the solid. The crystallinity and the purity of the solid were therefore attested by the combination of those 5 techniques.

Table 1. Chemical composition and lattice parameters of $Mg_2Al\text{-}NO_3$ LDH NPs.

Chemical composition				**Lattice parameters**	
Molar ratio Mg/Al^{ICP}	**C (wt. %)**	**H (wt. %)**	**N (wt. %)**	**a (Å)**	**c (Å)**
2.01	<0.05	3.2	5.7	3.04	26.62

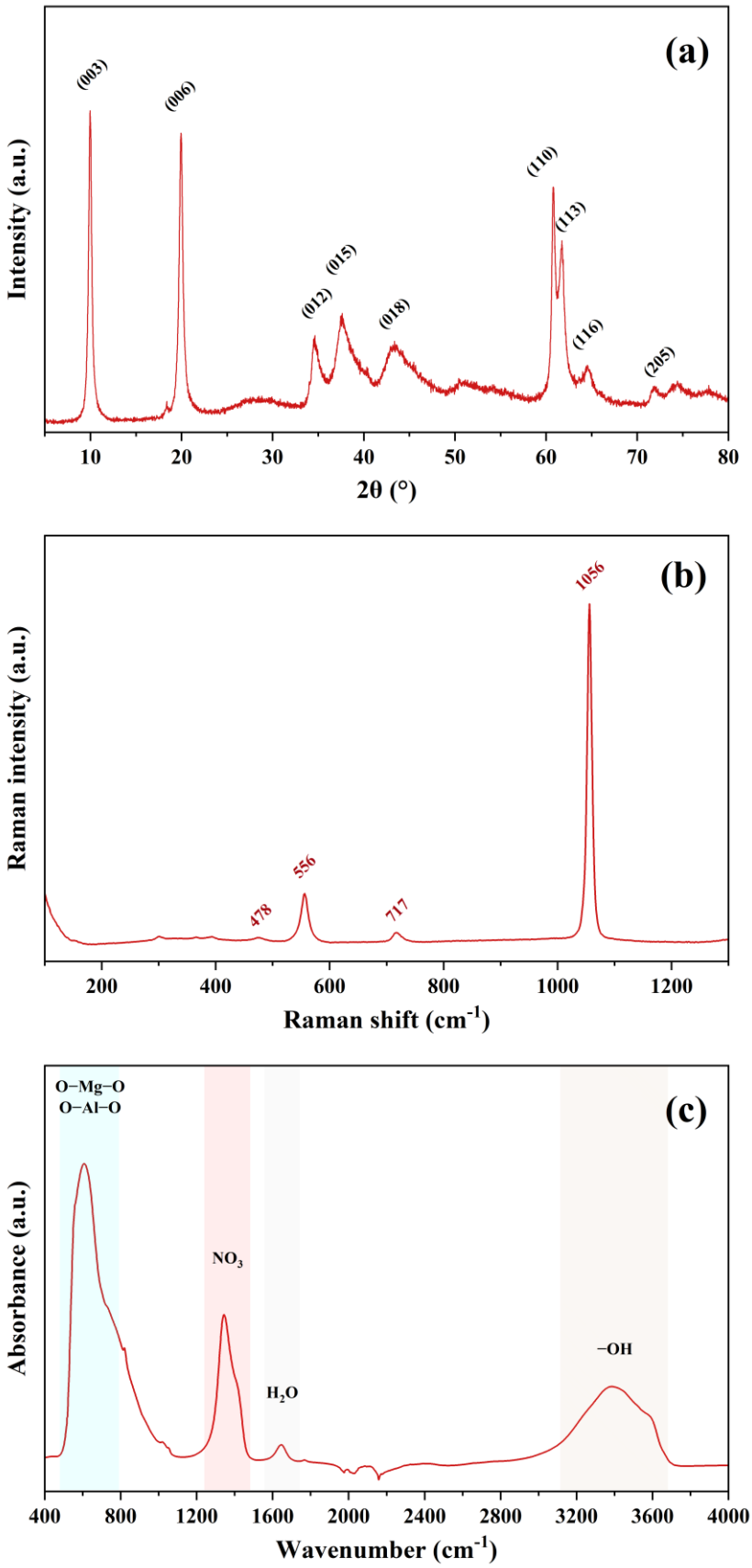

Figure 1: Structural characterization of LDH : (a) PXRD pattern of Mg_2Al-NO_3 NPs. (b) Raman spectra of Mg_2Al-NO_3 NPs. (c) FT-IR spectra of Mg_2Al-NO_3 NPs.

b. Particles dimensions

To be able to understand the interactions between Cr(VI) and the LDH, small particles with a narrow size distribution were needed to get uniform and quick interactions.

The analysis of particle size distribution by DLS as shown in Figure 2a unveiled a relatively narrow monomodal distribution of hydrodynamic diameter particles. The polydispersity index (PI), calculated as $PI = \frac{\sigma(l)^2}{\bar{l}^2}$, was serving as a measure of sample heterogeneity using the mean size (l) and the standard deviation of the size $\sigma(l)$ (Mudalige et al., 2019). In the case of LDH NPs, it exhibited a notably low value of approximately 0.13, reflecting a uniform and well-defined particle size distribution. Additionally, specific percentiles, namely D_{v10}, D_{v50}, and D_{v90}, corresponded to the diameters below 10%, 50%, and 90% of the particles population. The median diameter, D_{v50}, measured at 185 ± 25 nm and the D_{v90} was at 327 ± 13 nm. On the other hand, considering the 2D feature of LDH materials, while DLS assumed a spherical particle, the equation established by Lotya et al. (Lotya et al., 2013) suggested that the D_{v50} was 176 ± 8 nm.

SEM was employed to investigate the morphological characteristics, real-average diameter, and overall uniformity of the LDH NPs (Wani et al., 2021). As depicted in Figure 2b, SEM analysis confirmed the overall homogeneity of the NPs, even in their dry state. Specifically, the median diameter D_{50} measured at 133 ± 39 nm, while the diameter D_{90} found to be 183 ± 19 nm. Considering that the SEM give results on the number of dried particles and DLS results were given by the diffusion volume of hydrated particles and therefore a larger size, we assume that these results were in very good consistency.

AFM analysis employed to assess the height of the LDH NPs (Figure 2d) (Awassa et al., 2022). The resulting height profile unveiled a consistent and uniform average thickness of 22 nm (Figure 2e), specifically for $Mg_2Al\text{-}NO_3$ LDH NPs. This agreed with what was observed in SEM with some particles oriented with the layers perpendicular to the surface. This uniformity strongly indicated the multilamellar nature of the synthesized NPs, comprising approximately 25 layers in their structural composition.

The median size in the dimensions parallel to the layers was approximately 140 nm, as confirmed by both DLS and SEM. Moreover, the height (z-dimension) of the particles was consistently below 100 nm. The nomenclature "NPs" (colloidal Nano-Particles) aptly captures their size.

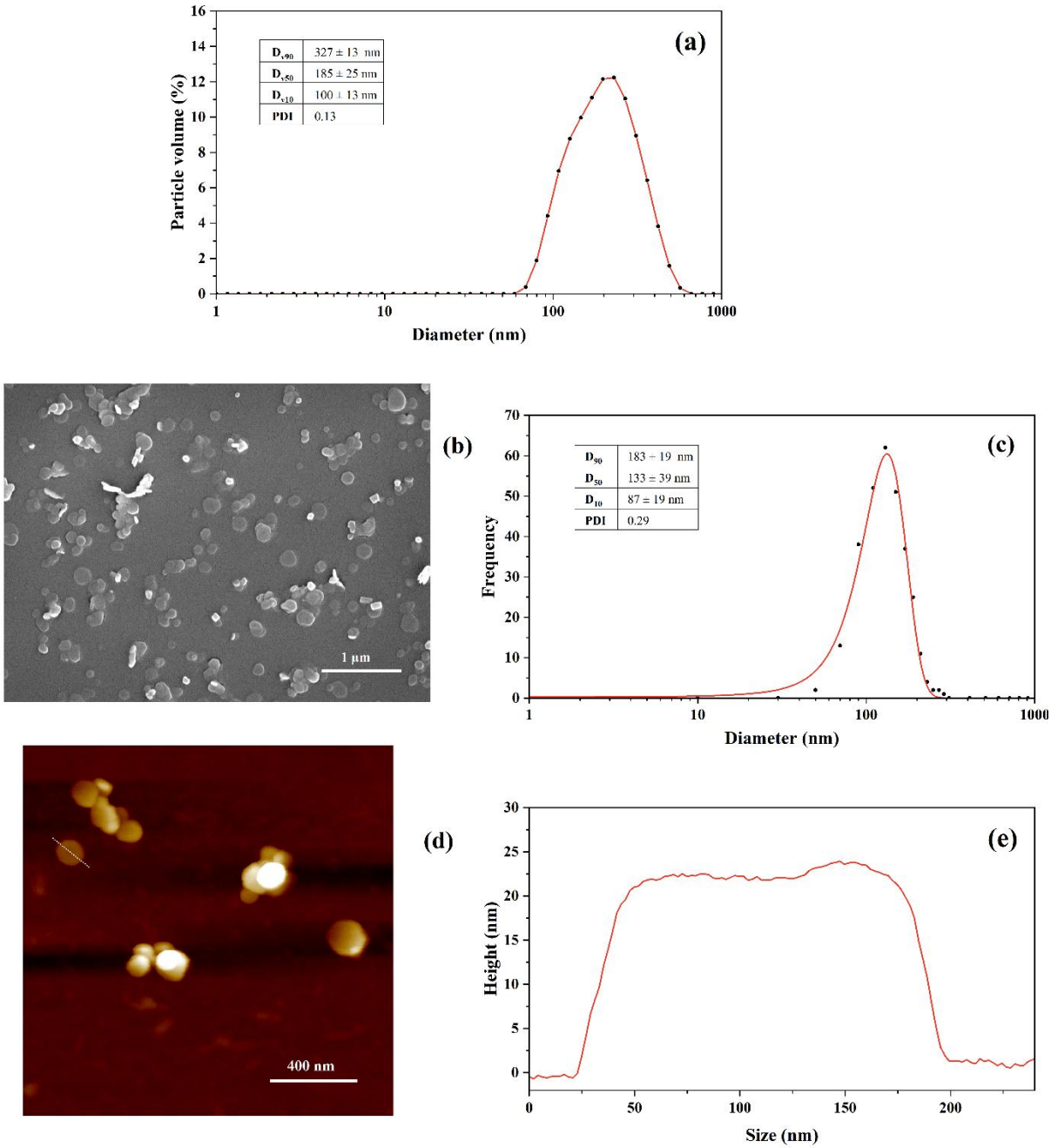

Figure 2: Morphological characterization of LDH : (a) DLS distribution analysis of $Mg_2Al\text{-}NO_3$ NPs. (b) SEM image of $Mg_2Al\text{-}NO_3$ NPs. (c) with its particle's size distribution. (d) AFM image of $Mg_2Al\text{-}NO_3$ NPs along with the height profile (e) of the disaggregated particle with dashed line.

c. Surface properties

The zeta potential had been measured and are shown on Figure 3 as a function of pH in the surrounding environment. Within the pH range of 4 to 8, these NPs demonstrated a constant zeta potential, maintaining a high positive value of approximately +50 mV. This relatively high electrophoretic potential explains the good stability of the colloidal suspension of the LDH NPs within this pH range. However, there was a decline in zeta potential between pH = 4 and pH = 2. This decrease in electrophoretic mobility can be attributed to partial neutralization of the hydroxide

constituting the solid, potentially leading to the dissolution of the LDH structure under these acidic conditions. Furthermore, beyond a pH of 9, there was another noteworthy trend: a gradual decrease in zeta potential. This decrease suggested the initiation of particle aggregation, which can negatively impact the stability of the colloidal system. The isoelectric point almost attained when the pH reaches 12. These results based on zeta potential analysis of the LDH NPs, conform to the reported surface characteristic of the LDH materials, where its surface was positively charged (Kumar et al., 2017; Li et al., 2009; Ouyang et al., 2021).

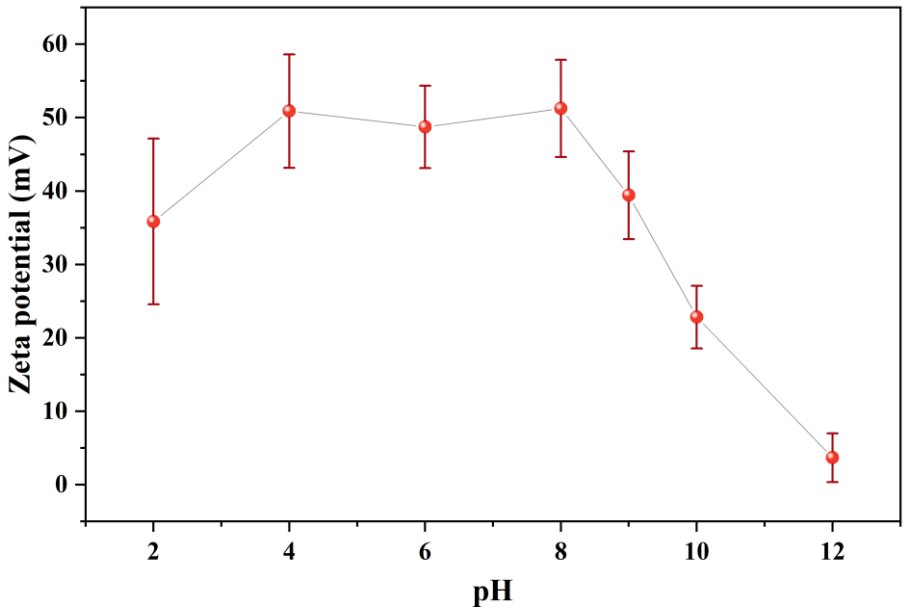

Figure 3: Zeta potential of Mg_2Al-NO_3 LDH NPs as a function of pH. c_{LDH} = 40 mg L^{-1} in ultrapure water. pH adjusted by NaOH and HNO_3.

2. Reactivity of the LDH towards Cr(VI):

a. UV-Vis spectrophotometry

The speciation of Cr(VI) was analyzed using UV-Vis spectrophotometry to determine the absorption coefficient for each ionic form. In Figure S2, the absorbance difference of Cr(VI) at both pH conditions revealed distinct forms: at pH = 4, the maximum absorption band at 350 nm indicates hydrogen chromate ion ($HCrO_4^-$), while at pH = 9, a shift to 375 nm corresponds to the basic form of Cr(VI), chromate ion (CrO_4^{2-}) (Szabó et al., 2018). Figure S3 displays the recorded absorption at the highest band absorptivity for each Cr(VI) form. The absorption coefficient at pH = 4 found to be 3.0 × 10^{-2} $L.cm^{-1}.mg^{-1}$, whereas at pH = 9, it was higher at 8.8 × 10^{-2} $L.cm^{-1}.mg^{-1}$. At low concentrations (under 100 mg L^{-1}), with a pKa of 6.5 (Tandon et al., 1984), $HCrO_4^-$ is predominant in acidic conditions (around pH = 4), while CrO_4^{2-} is predominant in alkaline conditions (pH = 9), resulting in different extinction behaviors.

The preliminary investigation involved comparing the half of the sum of the optical densities of the Cr(VI) solution and LDH suspension (The zero-time absorbance (A_0) spectrum) with the mixture of these solutions once equilibrated. At pH=9 (Figure S4a), there was an increase in optical density with a slight shift in wavelength. At pH=4 (Figure S4b), the increase and the wavelength shift were more pronounced than at pH=9. Interestingly, it revealed that the final absorbance of the mixture was almost the same at both pH. In the following paragraph, we described the stopped-flow study conducted to explore the interaction of Cr(VI) as a function of time.

b. Kinetic study using stopped-flow

The stopped-flow technique utilized to examine the interaction dynamics between LDH NPs and Cr(VI) at both pH = 4 and pH = 9. Based on the findings from a spectrophotometric preliminary study, a wavelength of 375 nm selected for the stopped-flow investigation. In a standard stopped-flow experiment, equal volumes of Cr(VI) solution with a specified concentration and an LDH suspension (0.25 g L^{-1}) were mixed, both with their pH adjusted to either 4 or 9. The zero-time absorbance (A_0) readily determined as the average of the initial absorbances of the two solutions. This is illustrated in Figure S5, providing an example at pH = 4. If there were no reaction, the absorbance would remained constant at this value.

In Figure S5 (for the first 50 ms) and 4 (lasting 50 s), the absorbance variations resulting from the combination of $HCrO_4^-$ and LDH NPs under acidic conditions (pH = 4) are visually depicted. This graph confirms the substantial absorbance changes noted in the previous section through standard UV-Vis analysis. Notably, the primary observation was that a significant portion of the absorbance modification occurred within the stopped-flow mixing time, specifically below 5 milliseconds. and therefore, cannot be characterized using this technique. Following this rapid phase, all curves exhibited a consistent shape across different concentrations of $HCrO_4^-$. Similarly, the curves for various Cr(VI) concentrations share a resemblance, showing that the final absorbance variation after interaction was proportional to the initial Cr(VI) concentration. After the burst, the observed absorbance variation during the following 50 seconds had been analyzed by fitting the data to a range of classical kinetic models, including the Pseudo First Order, Pseudo Second Order, Vermeulen model, and an adapted shrinking core model proposed in a preceding work, as illustrated in Figure S6. The model that exhibited the most accurate fit to the data was one we previously developed and adapted for our study, which is a mathematical solution to the equation proposed by Helffrich, describing the shrinking core model of ionic species through a solid system (Helfferich et al., 1985) but without keeping constant the concentration in the solution. Specifically tailored to elucidate ion exchange kinetics on microparticles of ion exchange resins (Hébrant, 2007), the Eq. 1 representing this model when absorbance is measured as a function of time is stated as follows:

$$Abs\ (t) = (A_1 - A_e)\ \exp(-k_{obs}t^{0.5}) + A_e \quad (1)$$

The specific time-dependent dependence of absorbance, *Abs* (*t*), was attributed to a rate-limiting step governed by diffusion either in the aqueous layer surrounding the solid or within the solid itself. In this context, A_1 is the zero-time absorbance of the stopped-flow analysis, "$A_1 - A_e$" represents the amplitude of the change in absorbance, "k_{obs}" corresponds to the observed rate constant of the reaction, and "A_e" denotes the equilibrium absorbance.

The very first result of this kinetic study was that the adsorption, which is an ion exchange reaction, occurs in two steps. The very fast initial phase, occurring within the first milliseconds, in which a quick jump of the optical density representing up to 80% of the total variation. This phase was too quick to be analyzed by the stopped-flow technique, given that the reaction order may reach 10^6 s^{-1} (Gomez-Hens and Perez-Bendito, 1991; Kobayashi et al., 1982), followed by a slower process which can be described by the Eq. 1. The variations cannot be attributed to a pH change, as the pH of both solutions is adjusted just before mixing and the pH of the remaining liquid, analyzed after mixing, is still 4. Our hypothesis posits that the initial change in absorbance was attributed to two simultaneous modifications. The First was the deprotonation of the $HCrO_4^-$ ion which occurs in the vicinity of the particles, likely at a higher pH than the surrounding bulk solution, thereby altering the absorption properties of this species. The second was the attenuation coefficient of chromate which undergoes modification upon adsorption to the surface due to the strong electrostatic attraction between Cr(VI) anions and the positively charged surface. This interaction involved approximately 10% of the active sites, a calculation based on the available Al atoms (Hsu et al., 2019), with a specific emphasis on the external active sites. Although this percentage may seem relatively low, it implies that electrostatic attraction and anion exchange operate simultaneously, collectively contributing to 80% of the total variation observed. This phenomenon has a low barrier energy of adsorption. After this fast initial phase, the subsequent change, as described by Eq. 1, was linked to the diffusion of species within the aqueous layer surrounding the LDH NPs or the intraparticle diffusion of Cr(VI) into the LDH interlayer space. This correlation was supported by the fact that the Intraparticle Diffusion model aligns well with the observed variation.

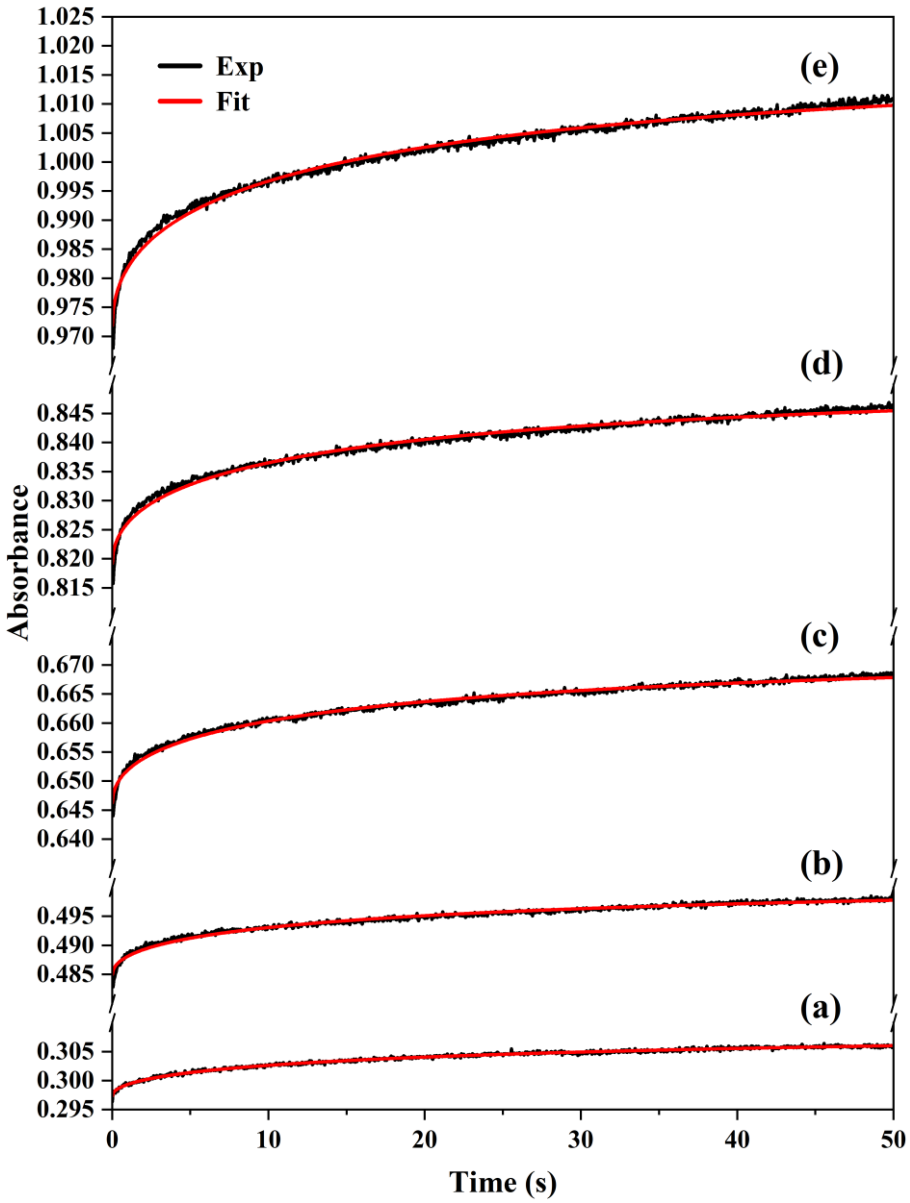

Figure 4: The stopped-flow plots at pH = 4 at different Cr(VI) concentrations (a): 2.5 mg L^{-1}, (b): 5.0 mg L^{-1}, (c): 7.5 mg L^{-1}, (d): 10.0 mg L^{-1}, (e): 12.5 mg L^{-1}. $[LDH]_0$ = 0.25 g L^{-1}.

A very similar trend observed in alkaline media (Figure S7). As the concentration of Cr(VI) increased, there was a gradual rise in the relative variation under both conditions. Interestingly, the final *Abs* (*t*) values were nearly identical in both pH. In this scenario, the deprotonation of the $HCrO_4^-$ ion cannot account for the rapid change in absorbance. The initial rapid step represents a lower proportion of the total absorbance variation at pH = 9 than at pH = 4. Instead, the rapid initial change was attributed to electrostatic adsorption to the surface, while the subsequent slower step involved diffusion towards and within the particle. These two mechanisms contribute to the observed variation.

The parameters obtained from the fitting procedure are compiled in Table S2a and S2b and are presented in Figure 5. In absolute value the $(A_1 - A_e)$ absorbance was proportional to the Cr(VI) concentration (Figure 5a). In contrast, the k_{obs}, which is the rate constant of the reaction occurring

during the interaction with the LDH surface, showed relatively constant values, regardless of the Cr(VI) concentration in the range explored here and the pH conditions with an average k_{obs} of approximately 0.25 $s^{-0.5}$ (Figure 5b), which implies an unchanged nature of the interaction phenomenon with LDH NPs at both pH and various concentrations. Notably, this value closely aligns with the value of 1 $s^{-0.5}$ found during investigations into simple ion exchange on synthetic resins (Hébrant, 2007). Finally, the final absorbance state, represented by A_e, was equal for the same initial Cr(VI) concentration in both pH conditions (Figure 5c). This suggested that the concluding state of Cr(VI) after interaction with the LDH surface remains unaltered regardless of pH conditions. Despite the pH disparity and the resulting difference in charge, there was no significant distinction in the kinetic results. The independence of the slow part of the ion exchange process from pH, coupled with its relatively moderate speed within the same timeframe as ion exchange on synthetic commercial resins, challenges the likelihood of a dissolution/reformation mechanism that was observed for phosphate incorporation (Kim et al., 2020).

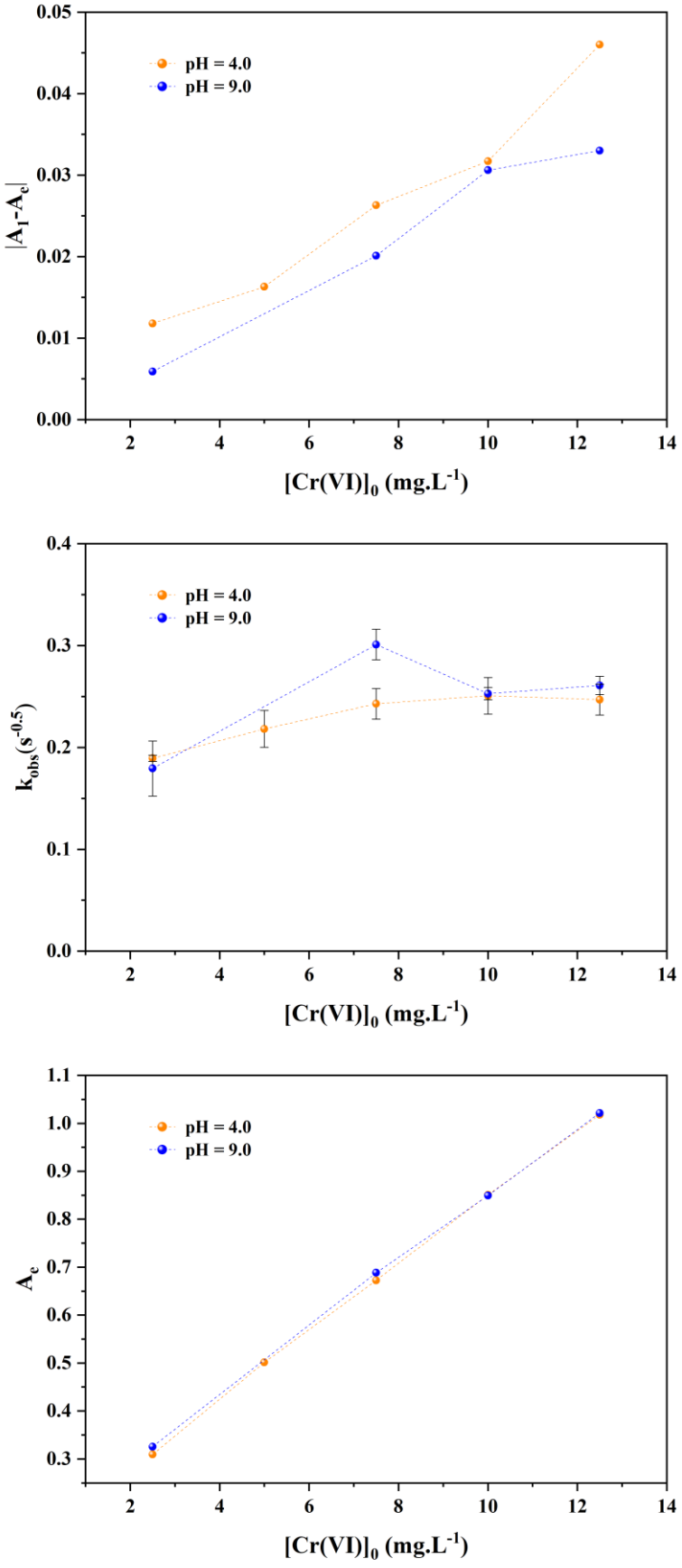

Figure 5: Fitted parameters values as a function of Cr(VI) concentrations at both pH conditions.

c. Thermodynamics using ultrafiltration

Figure 6 a and b indicate the extraction yield was defined on the basis of Cr elemental ICP-MS analysis of the permeate. This yield was calculated as:

$$Y\ (\%) = 100 \times \left(\frac{[Cr]_0 - [Cr]_{Permeate}}{[Cr]_0} \right) \quad (2)$$

With $[Cr]_0$ indicating the initial concentration and $[Cr]_{permeate}$ the concentration in the permeate.

We acquired two sets of data : Figure 6a in which the adsorbent concentration varied within the range of 0.05 to 0.5 g L^{-1}, while maintaining a constant Cr(VI) concentration of 7.5 mg L^{-1}. This variation allowed for the assessment of the NPs' extraction efficiency. In the second set of experiments Figure 6b, adsorption isotherms had been established by subjecting an LDH NPs suspension with a fixed concentration of 0.25 g L^{-1} to various Cr(VI) solutions ranging from 2.5 to 100 mg L^{-1}.

For a fixed Cr(VI) concentration (Figure 6a), at both pH levels, the extraction efficiency reached a plateau at around 0.10 - 0.15 g L^{-1} of LDH, indicating up to 99.9% extraction of chromium from the solution. This suggested an approximate capacity to fix approximately 225.1 $mg.g^{-1}$ of chromate, highlighting the highly favorable nature of anion exchange for chromate, this indicated that a residue of less than 10 ppb was achieved with this system, meeting the WHO standard of 50 ppb for total Cr. At very low LDH content and pH = 9, the extraction efficiency started at 57.5%, higher than in acidic conditions, decreases before re-increasing. A similar trend, albeit at a smaller scale, was observed at pH = 4. This counterintuitive phenomenon, where a larger adsorption occurs with a smaller quantity of LDH, may be attributed to the Donnan membrane effect (Hébrant, 2009; Tounissou et al., 1996). The slightly negatively charged membrane groups repels chromate ions, particularly at very low LDH concentrations, owing to the low ionic force in the solution (the only salt in solution was the chromate at 0.15 mmol L^{-1}). We intentionally avoided adjusting or buffering the ionic strength to prevent any interference in the anion exchange process.

In Figure 6b, the variation in Cr concentration at a constant LDH concentration revealed a consistently high extraction efficiency, averaging up to 99.9%, for Cr concentrations below 15 mg L^{-1} at both tested pH values. However, as the Cr concentration increased, the LDH exchange capacity was overpassed, and the extraction logically gradually decreased to approximately 36% at pH = 4 and 43.3% at pH = 9 when the concentration reaches 60 mg L^{-1}. Beyond this concentration, the extraction continued to decrease slowly, indicating that the LDH material was fully saturated. Included on both Figure 6, the points A and B represented the same experiment.

Since $HCrO_4^-$ predominates at pH = 4 and CrO_4^{2-} at pH = 9, if the ion exchange reaction is governed by a stochiometric process on the electric charges of the implied ions, one nitrate can be released when

462 one $HCrO_4^-$ is fixed and 2 nitrate ions can be exchanged for one CrO_4^{2-}. This led us to a priori consider
463 two different reactions :

$$NO_{3\,LDH}^- + HCrO_{4\,W}^- = NO_{3\,W}^- + HCrO_{4\,LDH}^- \quad (3)$$

464

465 At pH = 4, and

$$2NO_{3\,LDH}^- + CrO_{4\,W}^{2-} = 2NO_{3\,W}^- + CrO_{4\,LDH}^{2-} \quad (4)$$

466

467 At pH = 9, "W" indicates that the ion is in solution, and "LDH" indicates that it is within the LDH.
468 Reaction Eq. 4 was associated with the corresponding equilibrium constant :

$$K_9 = \frac{([NO_3^-]_W)^2 [CrO_4^{2-}]_{LDH}}{([NO_3^-]_{LDH})^2 [CrO_4^{2-}]_W} \quad (5)$$

469 In our case, as seen in the previous section, the final status seemed to be similar at pH = 4 and pH = 9.
470 Indeed, the ion exchanger is a layered double hydroxide, and the exchanger core is basic by nature
471 whatever the pH in the surrounding aqueous phase. Instead of reaction Eq. 3 we thus considered that
472 $HCrO_{4\,W}^-$ deprotonates at the proximity of the LDH:

$$2NO_{3\,LDH}^- + HCrO_{4\,W}^- = 2NO_{3\,W}^- + CrO_{4\,LDH}^{2-} + H^+{}_W \quad (6)$$

473 With its constant :

$$K_4 = \frac{([NO_3^-]_W)^2 [CrO_4^{2-}]_{LDH} [H^+]_W}{([NO_3^-]_{LDH})^2 [CrO_4^{2-}]_W} \quad (7)$$

474 As for the stopped-flow, we observed experimentally that the pH was not varying significantly during
475 the reaction : the pH of both reactants, adjusted at the same value by nitric acid initially, changes by
476 less of 0.1 unit during the reaction. This did not indicate that no proton was released during the
477 exchange but that the LDH particles were buffering the pH.

478 $[Cr]_W$ assumed to be determined by the permeate concentration and $[Cr]_{LDH}$ obtained by the mass
479 balance equation. The number of moles of LDH dispersed in the suspension is given by the mass of
480 LDH divided by its "molar mass" assuming an initial stoichiometry $Mg_2Al(OH)_6NO_3.1H_2O$. The pH
481 being adjusted by adding nitric acid, the initial nitrate concentration in the surrounding solution was
482 calculated as $[NO_3^-]_{W_0} = 10^{-pH}$. Although the LDH constitutes a separate phase we expressed the
483 concentrations of all species as their numbers of moles divided by the overall volume whatever the

phase in which they stand, The concentrations were low enough to be considered negligible in our calculations for the activity coefficients. K_9 may be then expressed as:

$$K_9 = \frac{\left([NO_3^-]_0 + 2[Cr]_0\left(\frac{Y(\%)}{100}\right)\right)^2 \left[[Cr]_0\left(\frac{Y(\%)}{100}\right)\right]}{\left([LDH]_0 - 2[Cr]_0\left(\frac{Y(\%)}{100}\right)\right)^2 \left[[Cr]_0\left(1 - \frac{Y(\%)}{100}\right)\right]} \quad (8)$$

Using a nonlinear least square fitting procedure (see SI for details), using this Eq. 7 we were able to fit Y (%) variation as a function of $[LDH]_0$ or $[Cr]_0$ variation.

On Figure 6, an additional dashed red line was introduced to illustrate the hypothetical scenario if NO_3^- were completely exchanged with $HCrO_4^-$ in the solution, following a 1:1 exchange as described in Eq. 3. Conversely, the dashed green curve represented a 2:1 exchange, where two nitrate ions were exchanged for one chromate, as per Eq. 6.

To derive the equation characterizing the exchange and equilibrium constant at pH = 4, two equations are used to fit with varying K constants as adjustable parameters. The obtained best fitting results in coefficients of determination (R^2) of 0.99 and 0.98 for LDH variation and Cr(VI) variation, respectively. This fitting corresponded to an exchange reaction of 2:1 LDH:Cr(VI) illustrated by Eq. 5, with the determined K_4 value being $7.07\times 10^{-3} \pm 0.69 \times 10^{-3}$. Conversely, at pH = 9, the R^2 for LDH variation was slightly lower than that in acidic conditions, measuring at 0.95 due to the emergence of the membrane effect. However, the R^2 for Cr(VI) variation remains approximately the same at 0.98. The equilibrium constant under alkaline conditions found to be higher than that under acidic conditions, K_9 determined to be 35.5 ± 2.7. However, this was linked to the introduction of the protonic concentration in Eq. 7, but the overall extractions were similar.

As outlined previously, our methodology for determining equilibrium constants differs slightly from conventional formulas such as the one proposed by Gaines and Thomas (Gaines and Thomas, 2004). By considering Eq. 4, which characterizes the reaction in question, we can derive the apparent equilibrium reaction constant $K_{NO_3^-}^{CrO_4^{2-}}$ as follows:

$$K_{NO_3^-}^{CrO_4^{2-}} = \frac{\gamma_{CrO_4^{2-}}[CrO_4^{2-}]_W (N_{NO_3^-})^2}{(\gamma_{NO_3^-})^2 [NO_3^-]_{LDH} N_{CrO_4^{2-}}} \quad (9)$$

Here, $\gamma(CrO_4^{2-})$ and $\gamma(NO_3^-)$ represent the solution-phase activity coefficients, while $N(NO_3^-)$ and $N(CrO_4^{2-})$ denote the LDH-phase activity in terms of mole fraction. The ion exchange constant (K_{ex}) can then be calculated from the apparent equilibrium constant based on $K_{NO_3^-}^{CrO_4^{2-}}$:

$$K_{ex} = \int_0^1 ln\ K_{NO_3^-}^{CrO_4^{2-}}\ d(LDH) \quad (10)$$

Indeed, they considered the activity coefficients of species in both the solid and solution phases, while In our analysis, we assumed that the activity coefficient ratios of nitrate and chromate ions remain constant at each stage and thus compensate for any fluctuations. Additionally, the concentrations were sufficiently low to be considered as such in our calculations. The study by Miyata (Miyata, 1983) involved the determination of ion exchange constants using Gaines and Thomas approach for various series of anions using nitrated Mg/Al LDH. The K_{ex} in their study ranged from 0.3 to 26.3 for monovalent anions (OH^-, F^-, Cl^-, Br^-, and I^-) and was found to be 24.5 and 69.2 for bivalent anions (SO_4^{2-} and CO_3^{2-}). In a related context, Goh et al. (Goh et al., 2009) utilized nitrated Mg/Al LDH for arsenic removal, and their method of directly determining nitrate release contrasts with our indirect approach. In our study, nitrate release was inferred through the determination of the concentration of non-adsorbed Cr, yielding results similar to theirs with a K_{ex} value of 30.6. The convergence of these findings underscores the reliability of our results, particularly considering the similarity of the systems studied, such as chromate.

a)

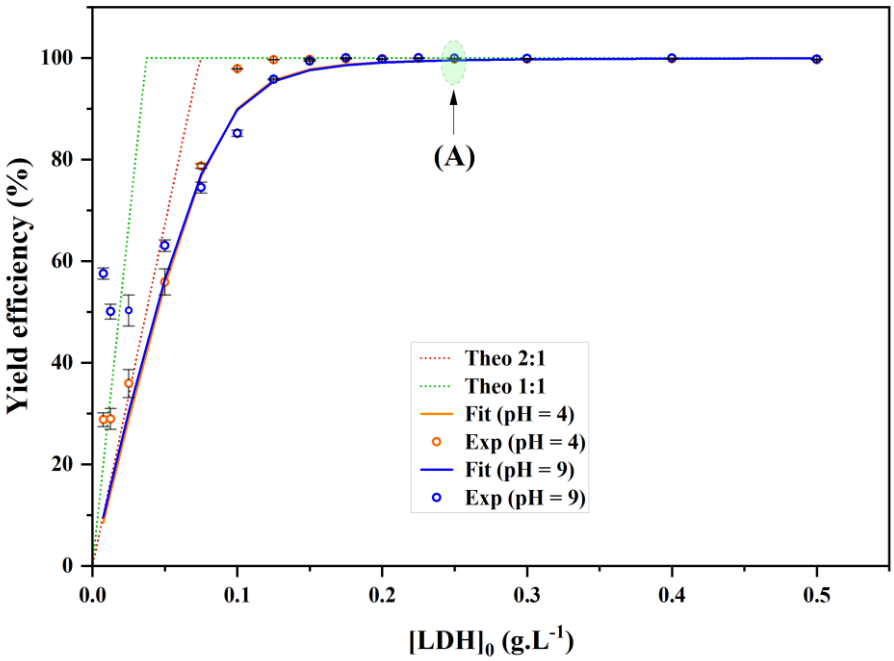

b)

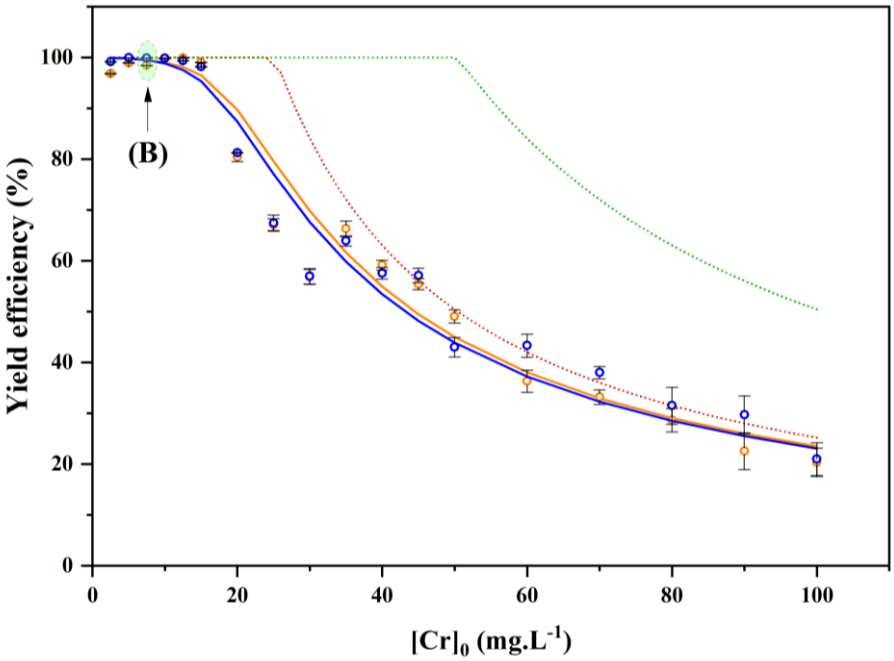

Figure 6: Yield of Cr ion extraction versus $[LDH]_0$ with fitted lines and experimental data points at both pH conditions, along with the theoretical curve at the 2:1 and 1:1 of LDH:Cr(VI) ratios (a). Yield of Cr ion extraction versus $[Cr]_0$ with fitted lines and experimental data points at both pH conditions, along with the theoretical curve at the 2:1 and 1:1 Cr(VI):LDH ratios (b).

Table 3: Thermodynamic reaction constants determined with mathematical fitting at both pH conditions.

pH	Concentration variation	R^2	K	σ(K)
4	LDH	0.993	7.07×10^{-3}	0.69×10^{-3}
	Cr	0.982		
9	LDH	0.956	35.5	2.7
	Cr	0.984		

To assess the structural changes resulting from the interaction with Cr(VI), PXRD analysis was employed, as depicted in Figure 7. The PXRD plot compared the crystallinity of LDH before and after interaction with Cr(VI). Interestingly, the LDH structure of the layers remains unchanged during the exchange at both pH levels, as evidenced by the unchanged (110) peak. However, there was a subtle shift observed in the (003) and (006) peaks. Notably, this shift corresponded to a reduction in the c, decreasing from 26.62 Å in unreacted LDH to 25.52 Å at pH = 4.0 and further to 24.85 Å at pH = 9.0, as detailed in Table 4. Additionally, the crystallite size, determined by the Full Width at Half Maximum (FWHM) of the peaks for LDH post-Cr(VI) interaction, exhibited a significant decrease. This was particularly evident in the reduced intensity and widening of the (003) and (006) reflections, indicating a substantial impact on the crystallinity factor of the final product. The crystallite size was reduced from 19.5 nm in the LDH reference, in agreement with the AFM measurement (Figure 2d) to approximately 10.5 nm at pH = 4 and 8.6 nm at pH = 9, further emphasizing the structural changes induced by the interaction with Cr(VI) and the diminished crystallinity domain in the c direction, while the crystallinity of the layers in the a and b directions remained unchanged, demonstrating once again the absence of a dissolution-recrystallisation path.

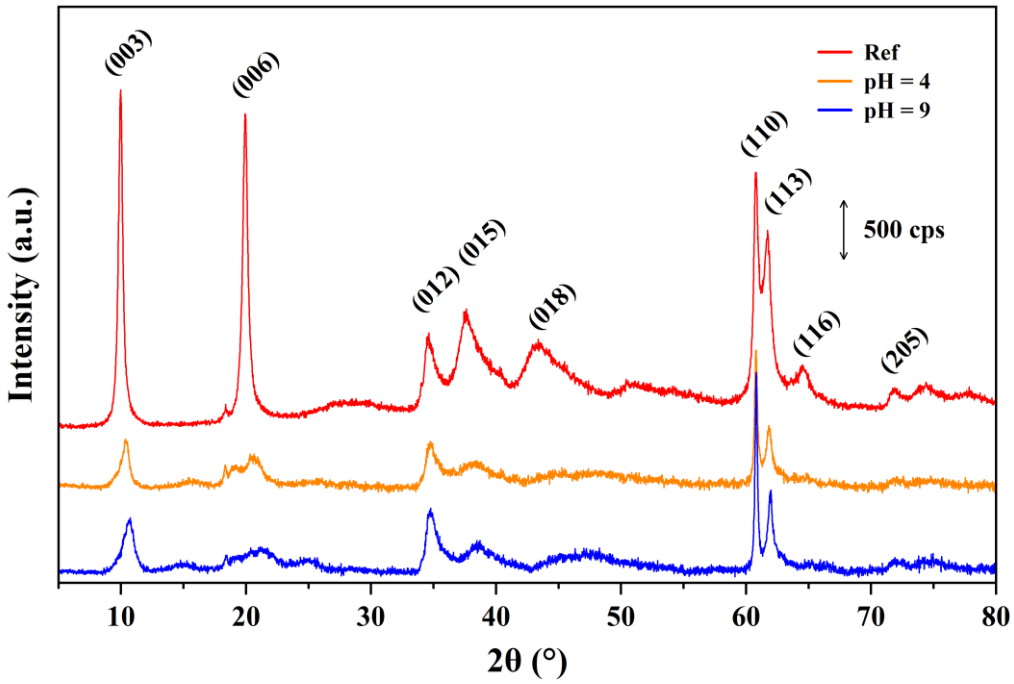

547

548 Figure 7: PXRD of LDH reference before adsorption, After adsorption at pH = 4, and after adsorption at pH = 9.

549

Table 4: Lattice parameters of LDH reference before adsorption, After adsorption at pH=9, and after adsorption at pH = 4.

Sample	$d_{(003)}$ (Å)	a (Å)	c (Å)	Crystallite Size (nm)
Reference sample	8.87	3.04	26.62	19.5
pH = 4.0	8.51	3.04	25.54	10.5
pH = 9.0	8.28	3.04	24.85	8.6

Conclusion.

This work provided a comprehensive investigation into the synthesis and characterization of the nitrate form of Mg/Al LDH NPs, covering their reproducible synthesis, structural properties, and colloidal behavior. The study delved into the reactivity of these LDH NPs towards Cr(VI) in colloidal state. Through the combination of colloidal state analysis and stopped-flow techniques, CrO_4^{2-} was the only anion incorporated into the LDH interlayer, with this process being pH-independent. The Cr(VI) adsorption process was elucidated into two distinct stages: rapid surface adsorption and deprotonation followed by interlayer diffusion, with the former occurring in less than 5 ms and the entire exchange process completed in 100 seconds. This was significantly faster than reported in existing literature in which mixing time and diffusion towards the particle were limiting the pace of the interaction. Interestingly, despite differing thermodynamic constants, the chromium extraction efficiency remains nearly identical at both pH values (4 and 9) considered in this study at equilibrium. The Mg/Al LDH NPs demonstrated the capacity to fix approximately 225.1 $mg.g^{-1}$ of chromate if considering the full exchange achieved in ultrafiltration tests. Nitrate strongly favors the exchange process, with up to 99.9 % of initially present nitrate ions shown to be exchangeable. Additionally, despite a reduction in crystallite size, the fundamental LDH structure remains unchanged during the exchange process. This research lays the foundation for future investigations into the application of LDH NPs in column conditioning for chromium extraction from dilute effluents containing other anions. The determination of anion exchange constants and the kinetic description presented herein will be vital parameters for further exploration in this direction.

Acknowledgement

CHNS elemental analysis was performed by Sandrine Adach on the SynBioN platform hosted by the L2CM. Raman, IR, UV-Vis, AFM, and SEM techniques were conducted on the SMI platform hosted in LCPME, while XRD results were obtained in the PMD2X platform hosted in CRM2. The ICP-MS was financed by a grant from FEDER SUSCHEMPROC, and the microwave oven was funded by an ICEL Carnot Grant. The authors express gratitude to Cédric Carteret for insightful discussions on Raman and FT-IR results, Pierrick Durand for his support in acquiring and analyzing XRD results, Claire Genois for assistance with ICP-MS, Aurelien Renard for help with SEM-EDX, and Abdessadek

579 Anagri for assistance with AFM measurements. The authors also acknowledge Samantha Soulé,
580 Christian Ruby, and Madjid Tarabet for their fruitful discussions.

Bibliography

Ahmed, M.A., Mohamed, A.A., 2023. A systematic review of layered double hydroxide-based materials for environmental remediation of heavy metals and dye pollutants. Inorganic Chemistry Communications 148, 110325. https://doi.org/10.1016/j.inoche.2022.110325

Awassa, J., Soulé, S., Cornu, D., Ruby, C., El-Kirat-Chatel, S., 2022. Understanding the role of surface interactions in the antibacterial activity of layered double hydroxide nanoparticles by atomic force microscopy. Nanoscale 14, 10335–10348. https://doi.org/10.1039/D2NR02395D

Barnhart, J., 1997. Occurrences, Uses, and Properties of Chromium. Regulatory Toxicology and Pharmacology 26, S3–S7. https://doi.org/10.1006/rtph.1997.1132

Bitetto, A.D., 2017. Étude structurale et dynamique d'hydroxydes doubles lamellaires: du matériau carbonaté aux hybrides organo-minéraux.

Chao, H.-P., Wang, Y.-C., Tran, H.N., 2018. Removal of hexavalent chromium from groundwater by Mg/Al-layered double hydroxides using characteristics of in-situ synthesis. Environmental Pollution 243, 620–629. https://doi.org/10.1016/j.envpol.2018.08.033

Chubar, N., 2011. New inorganic (an)ion exchangers based on Mg–Al hydrous oxides: (Alkoxide-free) sol–gel synthesis and characterisation. Journal of Colloid and Interface Science 357, 198–209. https://doi.org/10.1016/j.jcis.2011.01.098

Dong, Y., Kong, X., Luo, X., Wang, H., 2022. Adsorptive removal of heavy metal anions from water by layered double hydroxide: A review. Chemosphere 303, 134685. https://doi.org/10.1016/j.chemosphere.2022.134685

El Gaayda, J., Rachid, Y., Titchou, F.E., Barra, I., Hsini, A., Yap, P.-S., Oh, W.-D., Swanson, C., Hamdani, M., Akbour, R.A., 2023. Optimizing removal of chromium (VI) ions from water by coagulation process using central composite design: Effectiveness of grape seed as a green coagulant. Separation and Purification Technology 307, 122805. https://doi.org/10.1016/j.seppur.2022.122805

Feng, X., Long, R., Wang, L., Liu, C., Bai, Z., Liu, X., 2022. A review on heavy metal ions adsorption from water by layered double hydroxide and its composites. Separation and Purification Technology 284, 120099. https://doi.org/10.1016/j.seppur.2021.120099

Frost, R.L., Musumeci, A.W., 2006. Nitrate absorption through hydrotalcite reformation. Journal of Colloid and Interface Science 302, 203–206. https://doi.org/10.1016/j.jcis.2006.06.024

Gaines, G.L., Jr., Thomas, H.C., 2004. Adsorption Studies on Clay Minerals. II. A Formulation of the Thermodynamics of Exchange Adsorption. The Journal of Chemical Physics 21, 714–718. https://doi.org/10.1063/1.1698996

Goh, K.-H., Lim, T.-T., 2010. Influences of co-existing species on the sorption of toxic oxyanions from aqueous solution by nanocrystalline Mg/Al layered double hydroxide. Journal of Hazardous Materials 180, 401–408. https://doi.org/10.1016/j.jhazmat.2010.04.045

Goh, K.-H., Lim, T.-T., Banas, A., Dong, Z., 2010. Sorption characteristics and mechanisms of oxyanions and oxyhalides having different molecular properties on Mg/Al layered double hydroxide nanoparticles. Journal of Hazardous Materials 179, 818–827. https://doi.org/10.1016/j.jhazmat.2010.03.077

Goh, K.-H., Lim, T.-T., Dong, Z., 2009. Enhanced Arsenic Removal by Hydrothermally Treated Nanocrystalline Mg/Al Layered Double Hydroxide with Nitrate Intercalation. Environ. Sci. Technol. 43, 2537–2543. https://doi.org/10.1021/es802811n

Goh, K.-H., Lim, T.-T., Dong, Z., 2008. Application of layered double hydroxides for removal of oxyanions: A review. Water Research 42, 1343–1368. https://doi.org/10.1016/j.watres.2007.10.043

Gomez-Hens, A., Perez-Bendito, D., 1991. The stopped-flow technique in analytical chemistry. Analytica Chimica Acta 242, 147–177. https://doi.org/10.1016/0003-2670(91)87060-K

Guan, X., Yuan, X., Zhao, Y., Wang, Hou, Wang, Hui, Bai, J., Li, Y., 2022. Application of functionalized layered double hydroxides for heavy metal removal: A review. Science of The Total Environment 838, 155693. https://doi.org/10.1016/j.scitotenv.2022.155693

Hébrant, M., 2009. Metal ion extraction in microheterogeneous systems. Coordination Chemistry Reviews, Coordination Chemistry in Micelles 253, 2186–2192. https://doi.org/10.1016/j.ccr.2009.03.006

Hébrant, M., 2007. Conductivity stopped-flow study of the kinetics of solutes uptake by colloidal particles of synthetic resins. Journal of Colloid and Interface Science 311, 368–374. https://doi.org/10.1016/j.jcis.2007.03.029

Helfferich, F. g., Liberti, L., Petruzzelli, D., Passino, R., 1985. Anion Exchange Kinetics in Resins of High Selectivity. Part I. Analysis of Theoretical Models. Israel Journal of Chemistry 26, 3–7. https://doi.org/10.1002/ijch.198500061

Hsu, L.-C., Tzou, Y.-M., Chiang, P.-N., Fu, W.-M., Wang, M.-K., Teah, H.Y., Liu, Y.-T., 2019. Adsorption mechanisms of chromate and phosphate on hydrotalcite: A combination of macroscopic and spectroscopic studies. Environmental Pollution 247, 180–187. https://doi.org/10.1016/j.envpol.2019.01.012

Hsu, L.C., Wang, S.L., Tzou, Y.M., Lin, C.F., Chen, J.H., 2007. The removal and recovery of Cr(VI) by Li/Al layered double hydroxide (LDH). Journal of Hazardous Materials 142, 242–249. https://doi.org/10.1016/j.jhazmat.2006.08.024

Islam, Md.A., Angove, M.J., Morton, D.W., 2019. Recent innovative research on chromium (VI) adsorption mechanism. Environmental Nanotechnology, Monitoring & Management 12, 100267. https://doi.org/10.1016/j.enmm.2019.100267

Jarrah, N., Mu'azu, N.D., Zubair, M., Al-Harthi, M., 2020. Enhanced adsorptive performance of Cr(VI) onto layered double hydroxide-bentonite composite: Isotherm, kinetic and

thermodynamic studies. Separation Science and Technology 55, 1897–1909. https://doi.org/10.1080/01496395.2019.1614955

Kim, T.-H., Lundehøj, L., Nielsen, U.G., 2020. An investigation of the phosphate removal mechanism by MgFe layered double hydroxides. Applied Clay Science 189, 105521. https://doi.org/10.1016/j.clay.2020.105521

Kloprogge, J.T., Wharton, D., Hickey, L., Frost, R.L., 2002. Infrared and Raman study of interlayer anions CO32–, NO3–, SO42– and ClO4– in Mg/Al-hydrotalcite. American Mineralogist 87, 623–629. https://doi.org/10.2138/am-2002-5-604

Kobayashi, K., Tamura, M., Hayashi, K., 1982. Kinetic analysis of the recombination of nitric oxide with ferrihemoproteins by the flash photolysis method. Biochemistry 21, 729–732. https://doi.org/10.1021/bi00533a022

Kumar, N., Reddy, L., Parashar, V., Ngila, J.C., 2017. Controlled synthesis of microsheets of ZnAl layered double hydroxides hexagonal nanoplates for efficient removal of Cr(VI) ions and anionic dye from water. Journal of Environmental Chemical Engineering 5, 1718–1731. https://doi.org/10.1016/j.jece.2017.03.014

Lahkale, R., Sabbar, E., 2023. Impedance spectroscopy of solids for monitoring the adsorption kinetic of chromate ions from aqueous solution by a synthesized clay. Materials Today: Proceedings. https://doi.org/10.1016/j.matpr.2023.11.139

Lei, C., Zhu, X., Zhu, B., Jiang, C., Le, Y., Yu, J., 2017. Superb adsorption capacity of hierarchical calcined Ni/Mg/Al layered double hydroxides for Congo red and Cr(VI) ions. Journal of Hazardous Materials 321, 801–811. https://doi.org/10.1016/j.jhazmat.2016.09.070

Li, Y., Gao, B., Wu, T., Sun, D., Li, X., Wang, B., Lu, F., 2009. Hexavalent chromium removal from aqueous solution by adsorption on aluminum magnesium mixed hydroxide. Water Research 43, 3067–3075. https://doi.org/10.1016/j.watres.2009.04.008

Lotya, M., Rakovich, A., Donegan, J.F., Coleman, J.N., 2013. Measuring the lateral size of liquid-exfoliated nanosheets with dynamic light scattering. Nanotechnology 24, 265703. https://doi.org/10.1088/0957-4484/24/26/265703

Lv, X., Qin, X., Wang, K., Peng, Y., Wang, P., Jiang, G., 2019. Nanoscale zero valent iron supported on MgAl-LDH-decorated reduced graphene oxide: Enhanced performance in Cr(VI) removal, mechanism and regeneration. Journal of Hazardous Materials 373, 176–186. https://doi.org/10.1016/j.jhazmat.2019.03.091

Mantel, T., Glass, S., Usman, M., Lyberis, A., Filiz, V., Ernst, M., 2022. Adsorptive dead-end filtration for removal of Cr(VI) using novel amine modified polyacrylonitrile ultrafiltration membranes. Environ. Sci.: Water Res. Technol. 8, 2981–2993. https://doi.org/10.1039/D2EW00570K

Marappa, S., Radha, S., Kamath, P.V., 2013. Nitrate- Intercalated Layered Double Hydroxides – Structure Model, Order, and Disorder. Eur J Inorg Chem 2013, 2122–2128. https://doi.org/10.1002/ejic.201201405

690 Miao, J., Zhao, X., Zhang, Y.-X., Liu, Z.-H., 2021. Feasible synthesis of hierarchical porous MgAl-
691 borate LDHs functionalized Fe3O4@SiO2 magnetic microspheres with excellent adsorption
692 performance toward congo red and Cr(VI) pollutants. Journal of Alloys and Compounds 861,
693 157974. https://doi.org/10.1016/j.jallcom.2020.157974
694 Miyata, S., 1983. Anion-Exchange Properties of Hydrotalcite-Like Compounds. Clays Clay Miner. 31,
695 305–311. https://doi.org/10.1346/CCMN.1983.0310409
696 Mubarak, M., Jeon, H., Islam, Md.S., Yoon, C., Bae, J.-S., Hwang, S.-J., Choi, W.S., Lee, H.-J., 2018.
697 One-pot synthesis of layered double hydroxide hollow nanospheres with ultrafast removal
698 efficiency for heavy metal ions and organic contaminants. Chemosphere 201, 676–686.
699 https://doi.org/10.1016/j.chemosphere.2018.03.046
700 Mudalige, T., Qu, H., Van Haute, D., Ansar, S.M., Paredes, A., Ingle, T., 2019. Chapter 11 -
701 Characterization of Nanomaterials: Tools and Challenges, in: López Rubio, A., Fabra Rovira,
702 M.J., martínez Sanz, M., Gómez-Mascaraque, L.G. (Eds.), Nanomaterials for Food
703 Applications, Micro and Nano Technologies. Elsevier, pp. 313–353.
704 https://doi.org/10.1016/B978-0-12-814130-4.00011-7
705 Ouyang, Y., Xu, Y., Zhao, L., Deng, M., Yang, P., Peng, G., Ke, G., 2021. Preparation of ZnNiAl-
706 LDHs microspheres and their adsorption behavior and mechanism on U(VI). Sci Rep 11,
707 21625. https://doi.org/10.1038/s41598-021-01133-5
708 Qin, H., Hu, T., Zhai, Y., Lu, N., Aliyeva, J., 2020. The improved methods of heavy metals removal by
709 biosorbents: A review. Environmental Pollution 258, 113777.
710 https://doi.org/10.1016/j.envpol.2019.113777
711 Szabó, M., Kalmár, J., Ditrói, T., Bellér, G., Lente, G., Simic, N., Fábián, I., 2018. Equilibria and
712 kinetics of chromium(VI) speciation in aqueous solution – A comprehensive study from pH 2
713 to 11. Inorganica Chimica Acta, Special volume: dedicated to Professor Imre Sóvágó 472,
714 295–301. https://doi.org/10.1016/j.ica.2017.05.038
715 Tandon, R.K., Crisp, P.T., Ellis, J., Baker, R.S., 1984. Effect of pH on chromium(VI) species in
716 solution. Talanta 31, 227–228. https://doi.org/10.1016/0039-9140(84)80059-4
717 Tonomura, B., Nakatani, H., Ohnishi, M., Yamaguchi-Ito, J., Hiromi, K., 1978. Test reactions for a
718 stopped-flow apparatus: Reduction of 2,6-dichlorophenolindophenol and potassium
719 ferricyanide by l-ascorbic acid. Analytical Biochemistry 84, 370–383.
720 https://doi.org/10.1016/0003-2697(78)90054-4
721 Tounissou, P., Hebrant, M., Rodehuser, L., Tondre, C., 1996. Ultrafiltration of Micellar Solutions in
722 the Presence of Electrolytes. Journal of Colloid and Interface Science 183, 484–490.
723 https://doi.org/10.1006/jcis.1996.0571
724 Tran, H.N., Nguyen, D.T., Le, G.T., Tomul, F., Lima, E.C., Woo, S.H., Sarmah, A.K., Nguyen, H.Q.,
725 Nguyen, P.T., Nguyen, D.D., Nguyen, T.V., Vigneswaran, S., Vo, D.-V.N., Chao, H.-P., 2019.
726 Adsorption mechanism of hexavalent chromium onto layered double hydroxides-based

adsorbents: A systematic in-depth review. Journal of Hazardous Materials 373, 258–270. https://doi.org/10.1016/j.jhazmat.2019.03.018

Ukhurebor, K.E., Aigbe, U.O., Onyancha, R.B., Nwankwo, W., Osibote, O.A., Paumo, H.K., Ama, O.M., Adetunji, C.O., Siloko, I.U., 2021. Effect of hexavalent chromium on the environment and removal techniques: A review. Journal of Environmental Management 280, 111809. https://doi.org/10.1016/j.jenvman.2020.111809

Vaiopoulou, E., Gikas, P., 2020. Regulations for chromium emissions to the aquatic environment in Europe and elsewhere. Chemosphere 254, 126876. https://doi.org/10.1016/j.chemosphere.2020.126876

Verma, R., Sarkar, S., 2020. Trace Cr(VI) Removal: Evidence of Redox-Active Ion Exchange by a Weak-Base Anion Exchanger. Ind. Eng. Chem. Res. 59, 21187–21195. https://doi.org/10.1021/acs.iecr.0c04347

Wang, F., Guo, Z., 2019. Insitu growth of ZIF-8 on CoAl layered double hydroxide/carbon fiber composites for highly efficient absorptive removal of hexavalent chromium from aqueous solutions. Applied Clay Science 175, 115–123. https://doi.org/10.1016/j.clay.2019.04.013

Wani, A.A., Khan, A.M., Manea, Y.K., Salem, M.A.S., Shahadat, M., 2021. Selective adsorption and ultrafast fluorescent detection of Cr(VI) in wastewater using neodymium doped polyaniline supported layered double hydroxide nanocomposite. Journal of Hazardous Materials 416, 125754. https://doi.org/10.1016/j.jhazmat.2021.125754

Xie, B., Shan, C., Xu, Z., Li, X., Zhang, X., Chen, J., Pan, B., 2017. One-step removal of Cr(VI) at alkaline pH by UV/sulfite process: Reduction to Cr(III) and in situ Cr(III) precipitation. Chemical Engineering Journal 308, 791–797. https://doi.org/10.1016/j.cej.2016.09.123

Xu, Z.P., Zeng, H.C., 2001. Abrupt Structural Transformation in Hydrotalcite-like Compounds Mg1-xAlx(OH)2(NO3)x·nH2O as a Continuous Function of Nitrate Anions. J. Phys. Chem. B 105, 1743–1749. https://doi.org/10.1021/jp0029257

Yuan, X., Wang, Y., Wang, J., Zhou, C., Tang, Q., Rao, X., 2013. Calcined graphene/MgAl-layered double hydroxides for enhanced Cr(VI) removal. Chemical Engineering Journal 221, 204–213. https://doi.org/10.1016/j.cej.2013.01.090

Zhang, J.-W., Nur'aini, A.D., Wang, Y.-C., Hai, N.D., Van Minh, D., Chao, H.-P., 2022. Multiple pollutants removal by carbon sphere and layered double hydroxide composites: Adsorption behavior and mechanisms. Journal of Environmental Chemical Engineering 10, 108014. https://doi.org/10.1016/j.jece.2022.108014

Zhu, K., Gao, Y., Tan, X., Chen, C., 2016. Polyaniline-Modified Mg/Al Layered Double Hydroxide Composites and Their Application in Efficient Removal of Cr(VI). ACS Sustainable Chem. Eng. 4, 4361–4369. https://doi.org/10.1021/acssuschemeng.6b00922